Chain-Length Dependence of Optical Properties for an Alkanethiol Monolayer on an Ultrathin Gold Film Revealed via Reflected Light Microscopy

Hattori, Yoshiaki
Takahashi, Hayato
Ikematsu, Naoki
Kitamura, Masatoshi

(Citation)
Journal of Physical Chemistry C,125(27):14991-14999

(Issue Date)
2021-07-15

(Resource Type)
journal article

(Version)
Accepted Manuscript

Chain-length Dependence of Optical Properties for an Alkanethiol Monolayer on an Ultra-thin Gold Film Revealed via Reflected Light Microscopy

Yoshiaki Hattori[†*], *Hayato Takahashi*[†], *Naoki Ikematsu*[†], *and Masatoshi Kitamura*[†**]

[†]Department of Electrical and Electronic Engineering, Kobe University, 1-1, Rokkodai-cho, Nada, Kobe, 657-8501, Japan

Corresponding author:

*e-mail: hattori@eedept.kobe-u.ac.jp, **e-mail: kitamura@eedept.kobe-u.ac.jp

ABSTRACT:

In this work, a monolayer of *n*-alkanethiol formed on an approximately 8-nm-thick Au film, deposited onto a Si substrate with a thermally-grown SiO_2 layer, was characterized using reflected light microscope with a narrow band-pass filter. The semi-transparent, thin Au film, which is electrically conductive, provides interference in the films, and the optical properties of the monolayer depend on the alkanethiol length. When the surface of an Au film is photographed with a digital camera attached to the microscope, the color changes slightly with formation of a monolayer. The difference depends on the wavelength of a light source. Observations with the narrow band-pass filter of 490 and 520 nm were found to provide a large difference, which is useful to characterize a monolayer. The difference increases with the length of the alkyl chains in the monolayer. Thus, the presented approach enables the number of the alkyl chain units is identified through observations at an appropriate wavelength. This simple technique, which uses a general commercial microscope, can thus be used to confirm the presence of a monolayer with a molecular order thickness.

KEYWORDS: alkanethiol, monolayer, surface modification, optical microscopy, ellipsometry

INTRODUCTION

The modification of metal surfaces utilizing organic compounds containing sulfur has been widely studied for decades.[1, 2] Organic compounds chemically react on a metal surface and form a monolayer on it. This monolayer is useful for improving the performance of electronic devices,[3, 4] and fabricating nanosized materials and devices.[5–7] The properties of a monolayer, such as density, coverage, defects, homogeneity, and assembly order, depend on the preparation process and can affect the characteristics of an electronic device that is used. Therefore, a thorough characterization of monolayers is required for their application in electronic devices.[8] Monolayers formed on metal surfaces have been directly and indirectly characterized through various methods. Among the indirect methods, the following measurements of macroscopic properties have been conducted to evaluate the characteristics of monolayers: contact angle,[8–11] work function,[9] zeta potential,[8] and tolerance of chemical etching.[12] Among the direct methods, the elemental composition in monolayers has been investigated via X-ray photoelectron spectroscopy,[8, 9, 12–14] secondary ion mass spectrometry,[13] and Fourier-transform infrared spectroscopy.[10, 11, 13–17] In addition, the thickness of monolayers has been measured via X-ray reflectivity,[18] ellipsometry,[10, 11, 13, 15] and atomic force microscopy (AFM).[15, 19] Microscopic measurements of monolayers have been conducted via scanning electron microscopy[20] and AFM for patterning of the surface modification. Because individual methods are used for the evaluation of one or several properties, the combination of multiple methods play an important role in more in-depth investigation of the monolayer properties. In this sense, quick and simple techniques compatible with the practical processes used in electronics are still needed to evaluate the device performance when a monolayer is present.

Among various methods, optical measurements can be used to quickly evaluate a monolayer at atmospheric pressure with less damage. One of the most commonly used methods

is ellipsometry. Although ellipsometry is typically applied for evaluating nanometer-thick films, observing the in-plane distribution on the micrometer scale is difficult with this method. There are some techniques that enhance the ability to identify the presence of thin films. Traditionally, darkfield microscopy, differential interface-contrast microscopy, and phase-contrast microscopy with additional optical components are known to be capable of enhancing the contrast induced by the presence of a transparent thin specimen in a biological microscope. However, detecting the presence of a nanometer-thick film is usually difficult. In the 2000s, organic molecules on a thin metal film deposited onto a glass have been investigated by means of surface plasmon resonance.[17, 21] Similarly, surface-enhanced Raman spectroscopy has been used to detect the vibrational energy of organic molecules on a rough metal surface.[22, 23] However, these methods require the use of a transparent substrate and are thus not suitable for observation of organic molecules on a non-transparent Si substrate under visible light that represents the conditions generally used in electronics.

A simple optical method to visualize a nanometer-thick film on a Si substrate has been achieved by forming a SiO_2 layer onto the latter, with a thickness optimized to achieve interference. This method is widely applied in the research field of two-dimensional (2D) materials.[24] The intensity of the light reflected from a substrate is sensitive to the optical path inside the substrate. Thus, a thin film with an atomic thickness, such as graphene, on a substrate can be visualized using a standard reflected light microscope without any additional optical component. However, a ultra-thin film transparent to visible light, such as a monolayer of hexagonal boron nitride, does not provide sufficient contrast in the observation.[25] In addition, using an Au film under a thin film prevents interference because of its high optical reflectance.[26, 27] Therefore, other optical techniques are required for the visualization of a monolayer formed on a metal surface.

In this work, we report the characterization of a monolayer of *n*-alkanethiol, $CH_3(CH_2)_xSH$ with a chain length of x = 7–17, formed on a thin Au film deposited onto a SiO_2/Si substrate. The thin, semi-transparent Au film allows the incident light to interfere inside the SiO_2 layer. The interference contributes to enhancing the contrast induced by the presence of a thin film.[27] In the study, the monolayer was characterized using a standard reflected light microscope. The manuscript is organized as follows. First, the results of ellipsometry measurements conducted on substrates both with and without a monolayer are shown. The dependence of alkyl chain lengths and the influence of contamination on the substrate are discussed based on these findings. These results are used for discussing the optical images obtained via reflected light microscopy. Next, the images captured with an optical microscope using a digital camera through a narrow band-pass filter are shown. For the observation, two substrates, with and without a monolayer, were placed on the microscope stage side by side. The presence of the monolayer is discussed based on the intensity of the reflected light obtained in the form of digital data. The validity of the proposed method is evaluated through the comparison with the experimental data and numerical calculations. Finally, the method was applied for the observation of a monolayer formed from various *n*-alkanethiols.

EXPERIMENTAL METHODS

Preparation and characterization of monolayer

Si substrates with a thermally-grown, 91-nm-thick SiO_2 film were used in this study. The substrate was cleaned with an ultrasonic cleaner and UV/ozone irradiation. A 1.2-nm-thick MoO_x film and an Au film with a thickness of 4–16 nm were deposited via thermal evaporation with a quartz crystal microbalance (QCM) at a pressure of the order of 10^{-4} Pa at a rate of ~0.15 Å/s. The MoO_x film, which serves as an adhesive layer, is transparent in the visible light region

and is suitable for this optical study. The Au film with a thickness exceeding 6 nm was found to exhibit electrical conductivity (**Fig. S1**).[28] Typically, the sheet resistance of an 8-nm-thick Au substrate is 18 Ω/sq. The substrates were stored in N_2 (O_2 < 10 ppm, H_2O < 10 ppm) until being used for surface modification. To obtain a monolayer film, the substrate was immersed in an ethanol solution containing alkane thiol with molarity of 10^{-4} mol L^{-1} for 5 min at a room temperature in air.[29] The substrate was then rinsed with ethanol four times and dried with N_2 gas. Immediately after, the substrate was optically measured in air with a relative humidity of 30–50%. The measurement was performed using an ellipsometer (Auto SE, Horiba) and optical microscope (LV100, Nikon) equipped with either a monochrome 12-bit camera (CS-63M, Bitran) cooled down to 10 °C or a color 8-bit camera (EOS Kiss X4, Canon). 5× objective lenses with a numerical aperture (NA) of 0.15 (LU Plan 5 Flour 5×/0.15, Nikon) and 10× objective lenses with a NA of 0.30 (LU Plan Flour 10×/0.3, Nikon) were used for monochromatic and color images, respectively. A narrow band-pass filter was inserted in the optical path of the microscope just after the collector lens of the halogen lamp. The full width at half maximum (FWHM) of the narrow band-pass filters is 10 nm for 480–520 nm and ~35 nm for other wavelengths (λ). The condenser aperture diaphragm was adequately used. The morphological investigations were performed via AFM (NanoNavi, SII) in contact mode. The curvature of the AFM cantilever is about 20 nm. Alkane thiols, 1-octanethiol (C8, purity > 98%), 1-decanethiol (C10, purity > 95.0%), 1-undecanethiol (C11, purity > 96.0%), 1-dodecanethiol (C12, purity > 95.0%), 1-pentadecanethiol (C15, purity > 98.0%), 1-hexadecanetiol (C16, purity > 97.0%), and 1-octadecanethiol (C18, purity > 97.0%) were purchased from the Tokyo chemical industry and were used without further purification. In this study, a substrate with a monolayer formed from $CH_3(CH_2)_{n-1}SH$ (with n = 8, 10, 11, 12, 15, 16, and 18) is referred to as a Cn substrate.

Optical model

The multi-layered model is adopted for calculating the contrast in this study. The layer structure is composed of air, a monolayer, Au, MoO_x, SiO_2, and Si, numbered 0, 1, 2, 3, 4, and 5, respectively. d_j and N_j (= n_j+ ik_j; with j = 0, 1, …, 5 and i: imaginary unit) are the thickness and complex refractive index for the j-th layer, respectively. The refractive index of alkanethiol was assumed to be constant with respect to the wavelength, and N_1 was set to 1.475.[30] For the other layers, the experimentally-obtained refractive index was used for N_j (j = 2,..., 5).[31, 32] d_1 for the C12 and C18 monolayers was set to 1.1 and 2.2 nm, respectively.[30] d_2 and d_3 were set to the thickness values measured with a QCM. d_4 was set to the value determined via spectroscopic ellipsometry. For simplicity, the incident light was assumed to be perpendicular to the substrate surface, and the FWHM of the narrow band-pass filter was fixed at 10 nm. The reflectance (R=I_R/I_0) of the substrate with or without a monolayer was calculated using the Fresnel equation,[33] where I_0 and I_R are the intensity of the incident and reflected light, respectively. The I_0 was set to 1. Because the substrate was irradiated through a narrow band-pass filter with a central wavelength of λ' and a FWHM of about 10 nm, the reflectance of substrate detected by the camera, R'(λ'), was calculated according to:

$$R'(\lambda') = \frac{1}{10\ nm} \int_{\lambda'-5\ nm}^{\lambda'+5\ nm} R(\lambda) d\lambda.$$

The contrast compared with the experimental values was calculated by ($R'_{sample}(\lambda')$ − $R'_{ref}(\lambda')$)/$R'_{ref}(\lambda')$, where the subscript "sample" and "ref" stand for the substrate under the test and reference substrate, respectively.

RESULTS AND DISCUSSION

Firstly, the substrates without a monolayer were investigated via ellipsometry. In general, ellipsometry detects the light reflected from a substrate surface and provides the

coefficient $\rho = r_p/r_s = \tan \Psi \exp(i\Delta)$, where r_p and r_s are the reflection coefficients for p- and s-polarization, respectively. As an optical information of a substrate, wavelength-dependent Δ and Ψ are obtained. **Figures 1(a, b)** show Δ and Ψ, respectively, for substrates without a monolayer at an incidence angle of 70°. The three different types of black curves correspond to Δ and Ψ for the as-deposited substrates with an Au film with different thicknesses. The value of Δ at a specific wavelength increases upon increasing the Au thickness. By contrast, Ψ at a wavelength λ < 570 nm (> 570 nm) decreases (increases) upon increasing the Au thickness. This indicates that the thickness of the Au film influences the optical properties. Indeed, the color difference between the substrates can be easily confirmed with the naked eye. The color of the 16-nm-thick Au substrate is yellow, similar to that of a substrate with a thick Au film, whereas the color of the 4-nm-thick Au substrate is reddish. The red curves in **Figs. 1(a, b)** correspond to the Δ and Ψ values of a substrate that was immersed in ethanol without alkanethiol. The substrate not treated with alkanethiol was chosen for reference as substrates treated with ethanol containing alkanethiol are anyhow always rinsed with ethanol. A comparison between the black and red solid curves indicates that the immersion of a substrate in ethanol leads to a slight change in the Δ and Ψ values. It has been known that the Δ changes sensitively to an ultra-thin film on a substrate and, in particular, it decreases by the deposition of a film.[30] Thus, the change may be attributed to the removal of hydrocarbon molecules or water adsorbed onto the substrate.[34, 35, 36] This hypothesis is supported by the experimental results shown later. Thus, the substrate immersed in ethanol is here referred to as a bare Au substrate. Hereafter, Δ and Ψ for a bare Au substrate are denoted as Δ_{Au} and Ψ_{Au}, respectively.

Next, the substrate with a monolayer formed using *n*-alkanethiol was examined. **Figures 1(c, d)** show the spectra of $\delta\Delta = \Delta_{sample} - \Delta_{Au}$ and $\delta\Psi = \Psi_{sample} - \Psi_{Au}$, respectively. The black dashed and solid curves correspond to substrates with C18 and C10 monolayers, respectively. The red marks in the figures show the typical standard deviation of the error in

these measurements. The value of $\delta\Delta$ for both the C10 and C18 monolayers is negative, indicating that the formation of the C10 and C18 monolayers leads to a decrease in Δ. Additionally, $|\delta\Delta|$ for the C18 monolayer is larger than that for the C10 monolayer because of the longer alkyl chain present in the C18 monolayer. Furthermore, $\delta\Psi$ depends on the alkyl chains. Although the surface exhibits atomic order roughness, as can be seen in **Figs. 2(a, b)**, the difference in the alkyl chain length is reflected in the ellipsometry spectra because it is macroscopically observable. The fact that ellipsometry spectra depend on the alkyl chain length has also been reported in a previous study of C10 and C18 monolayers formed on 250-nm-thick Au films.[30, 37] The blue curves in **Figs. 1(c, d)** show the spectra of $\delta\Delta$ and $\delta\Psi$ for an as-deposited Au substrate, respectively. The Δ and Ψ values change by immersing the substrate in ethanol, which may be caused by the removal of hydrocarbon molecules or water adsorbed onto the substrate. [34, 35, 36]

Figures 2(a, b) shows the topological AFM images of the bare Au and C18 substrates, respectively, for 8-nm-thick Au. The insets are photographs of the water droplets on the substrates for measurements of the water contact angle. From the AFM images, it can be observed that the Au films exhibit a contiguous grain structure with a diameter of about 20 nm. The root mean square roughness estimated from the 1 μm × 1 μm images is 0.5 nm for both cases. Thus, the monolayer does not seem to affect the AMF images. A similar morphology has been observed for thermally-deposited Au films.[38] By contrast, the water contact angle depends on the substrate. The water contact angle for the C18 substrate is slightly higher than that for the as-deposited substrate. This indicates that the monolayer of the C18 substrate contributes to the increase in the water contact angle.[29]

The optical contribution of the monolayer was investigated using a microscope equipped with a narrow band-pass filter. A Si substrate was cleaved into two pieces before

being surface-treated. The two substrates were placed on the stage of the microscope and observed at the same time. **Figure 3(a)** shows the photograph of the bare Au and C18 substrates. Confirming the color difference between the two substrates with the naked eye is difficult. However, the color difference can be numerically obtained when the substrates are observed using a digital camera under controlled irradiation. **Figure 3(b)** is a schematic diagram to explain the cause of the difference later. **Figures 3 (c–g)** show the images of the 8-nm-thick Au substrates obtained from the 2D digital data (3072 px × 2048 px) acquired with the digital camera. Depending on the intensity of the light reflected from the substrate, D can have an integer value from 0 to 4095. The average value of the reflected light intensity depends on the substrate and observation conditions. Thus, the difference between D and the average of D (D_{ave}) is used to characterize the image of a substrate. This difference, $D - D_{ave}$, is represented by the blue-to-red color bar shown in **Fig. 3(c)**, which is applied to all images. Notably, the background noise, which can originate from different sources, including the camera and optical path, was numerically removed by subtracting the reference image (**Fig. S2**).

Figure 3(c) shows the image of an as-deposited substrate irradiated with light at λ = 490 nm; the number in the bottom-left corner of the figure is the D_{ave} value calculated from the D value of all pixels. A stripe pattern can be seen spanning the image from the top-right corner to the bottom-left corner. This pattern may be attributed to fluctuations in the thickness of the Au and/or MoO_x layers. The standard deviation of D for the substrate is 32.2, which is 1.3% of D_{ave}. The error corresponds to a thickness difference of ~0.01 nm for the MoO_x or Au film in later calculation. Note that the stripes were not observed when MoO_x is replaced with 0.5-nm-thick Cr film. **Figure 3(d)** shows the images of two substrate pieces obtained from a bare Au substrate through cleavage. The numbers in the bottom-left and bottom-right corners of the figure are the average D values obtained for the left and right substrate piece, respectively. The average value of the bare Au substrate is denoted as D_{Au}. The area of the contaminations caused

by cleavage was excluded from the calculation of D_{Au}. The stripe patterns for the left and right substrate pieces almost reproduce the pattern of the original substrate. The difference between the D_{Au} values is 19, which corresponds to about 1% of D_{Au}. **Figures 3(e–g)** illustrate the images of the bare Au and C18 substrates obtained from a substrate through cleavage. These images were obtained using band-pass filters for different λ values. The number in the bottom-right corner of the figure is the average of D for the C18 substrate, here denoted as D_{C18}. For observation using light with λ = 490 nm, D_{C18} was found to be larger than D_{Au}. Thus, the image for the C18 substrate has a reddish color. Conversely, D_{C18} was found to be smaller than D_{Au} for λ = 510 nm. Thus, the image for the C18 substrate has a bluish color. By contrast, D_{C18} is close to D_{Au} for λ = 500 nm.

The D value generally depends on the wavelength and observation conditions. Thus, the color difference should be discussed based on the relative difference $(D_{C18} - D_{Au})/D_{Au}$ rather than the absolute difference $(D_{C18} - D_{Au})$. The number in the bottom-center part of **Figs. 3(d–g)** indicates the value of the contrast, defined as $(D_{C18} - D_{Au})/D_{Au}$. It can be seen that the contrast values are 0.13, 0.02, and −0.10 for λ = 490, 500, and 510 nm, respectively. The dependence of the contrast on λ can be explained through the schematic diagram in **Fig. 3(b)**, which shows I_R as a function of wavelength. The I_R value is the smallest at a certain wavelength λ_{MIN}. From **Fig. 3(b)**, it can be observed that λ_{MIN} for the bare substrate is between 490 and 500 nm. The formation of a monolayer shifts the spectrum of I_R toward a higher wavelength. As a result, λ_{MIN} for the C18 substrate is between 500 and 510 nm. The difference between the I_R value for the bare substrate and C18 substrate is reflected by different colors in **Figs. 3(e–g)**. The wavelength dependence of the I_R is described in detail in **Fig. S3** in the Supplementary Information section.

The average value of D for a substrate, which is very sensitive to surface conditions, gradually changes even if the substrate is just placed in air. Thus, the time dependence of this value was also investigated quantitatively. **Figures 4(a, b)** show the time dependence of D_{Au} (gold) and D_{C18} (yellowish green) obtained for λ = 490 and 510 nm, respectively. The time t = 0 is defined as the moment at which the surface treatment process was completed. The halogen lamp in the microscope was turned on about 2 h before observation and was kept on. The power of the light under the objective lens was 9.7 μW/cm^2 just before observation and decreased by about 3% after observation. Thus, D_{Au} and D_{C18} values were calibrated based on the observed decrease. Here the light power is assumed to decreases linearly with time. In **Figs. 4(a, b)**, the orange and green curves represent the calibrated D_{Au} and D_{C18} values, respectively. The calibrated value is more suitable than the raw value for discussion. For both λ values, D_{Au} substantially changes more with time compared with D_{C18}. D_{Au} for λ = 490 and 510 nm gradually increases and decreases with time, respectively. Although the change in D_{C18} is very small, D_{C18} for λ = 490 nm slightly increases with time, whereas it decreases for λ = 510 nm. The reason of this trend is explained in **Fig. 4(c)**, which illustrates the schematic diagram of I_R for the bare Au and C18 substrates. The solid curves represent the I_R spectra for the initial state, whereas the dotted curves correspond to the I_R spectra after a certain amount of time. As time elapses, these spectra shift. The change in D_{Au} and D_{C18} seen in **Figs. 4(a, b)** corresponds to the arrows displayed in **Fig. 4(c)**. The change in D_{Au} and D_{C18} for λ = 500 nm (**Fig. S4**) is also explained in **Fig. 4(c)**. As discussed in the previous paragraph, deposits on a surface lead to a shift in the spectra toward higher wavelengths. The changes in D_{Au} and D_{C18} might be related to the adsorption of hydrocarbon molecules on the substrate. Because the change in D_{Au} is larger than that in D_{C18}, it is thought that hydrocarbon molecules are more easily absorbed on the bare Au substrate. In fact, the accumulation of the adsorption on Au film that occurs in

several tens of minutes in ambient environment has been indirectly investigated by measuring the water contact angle using a substrate immediately after Au deposition.[35]

The solid black curves in **Figs. 4(a, b)** illustrate the contrast between the substrates, namely, $(D_{C18} - D_{Au})/D_{Au}$. Notably, the reduction of irradiation power vanishes in the contrast, and the contrast is not affected by such reduction. For both wavelengths, the absolute value of the contrast decreases with time, indicating that the visibility of the C18 monolayer decreases with time. This means that the duration of a measurement needs to be carefully managed for quantitative comparisons of contrast. Regarding quantitative comparisons, the exposure time of the digital camera also affects the contrast, as long exposure times lead to a saturation of D. The determination of an appropriate exposure time is explained in **Fig. S5** in the Supplementary Information. Typical values of the exposure time for λ = 490 and 510 nm are 12.1 and 13.5 s, respectively.

Figure 5(a) shows the wavelength dependence of the contrast obtained from C18 substrates having Au films with different thicknesses. For all Au film thicknesses, the contrast values are positive (negative) in a range of distances shorter (longer) than the λ_0 wavelength, which is close to 500 nm. In other words, λ_0 is the wavelength at which the contrast is zero. In addition, it can be seen that the spectrum has a peak for $\lambda < \lambda_0$ and a valley for $\lambda > \lambda_0$. A similar wavelength dependence has been reported in the observation of thin 2D materials on Si/SiO_2 substrates without the Au film.[24, 25] Here, the wavelength at which the contrast is maximum (minimum) is denoted as λ_{MAX} (λ_{MIN}). The existence of λ_{MAX}, λ_0, and λ_{MIN} in the contrast spectrum was numerically confirmed, as explained in the next paragraph. The absolute value of the contrast for the 4- or 8-nm-thick Au film is larger than that for the 16-nm-thick Au. This indicates that utilizing an Au film with an appropriate thickness is an effective strategy for confirming the presence of a monolayer on the Au film.

To verify these experimental results, the contrast for the optical system shown in **Fig. 5(b)** was numerically calculated. For simplicity, the light assumed to be vertically incident on the substrate surface. The details of the calculation are described in the Methods section. **Figure 5(c)** presents the contour map of the contrast calculated as a function of the Au thickness and λ. For a certain Au thickness, there exists λ_{MAX}, $\lambda_{0,}$ and λ_{MIN}, which are represented by dotted red, blue, and black curves, respectively. To compare the experimental and calculated values, λ_{MAX}, $\lambda_{0,}$ and λ_{MIN} estimated from **Fig. 5(a)** are plotted in **Fig. 5(c)**. The plots for the 4-, 8-, and 16-nm-thick Au films have light-gold, gold, and dark-gold colors, respectively; circles, squares, and triangles denote λ_{MAX}, $\lambda_{0,}$ and λ_{MIN}, respectively. Although the plots do not exactly lie on the dotted curve, the dependence of the experimental λ_{MAX}, $\lambda_{0,}$ and λ_{MIN} on the thickness of the Au film can be roughly explained in terms of the contour map. On the contrary, the magnitude of the contrast derived from the experiment is different from that obtained through the calculation. However, calculation does not include the influence of oblique illumination through the objective lens, and incident light from multiple directions decreases the contrast.[39,] λ_{MAX}, $\lambda_{0,}$ and λ_{MIN} are also changed slightly with oblique illumination.[40] Thus, the assumption of vertical incidence may be the reason behind the discrepancy between the experimental and calculated contrast.

Monolayers with different alkyl chain lengths were also examined. A longer alkyl chain is expected to result in a larger contrast. For the experiment, in order to avoid the influence of the adsorption of the contamination onto the surface, the C12 substrate was used as a reference instead of the bare Au substrate. Substrates with an 8-nm-thick Au film were used for the experiment. Each substrate was cut into two pieces through cleavage; one piece was immersed in a solution of 1-dodecanethiol and the other was immersed in another thiol. The contrast for the substrate was measured in air within about 30 min of drying. **Figure 6(a)** shows the contrast, defined as $(D_{Cn} - D_{C12})/ D_{C12}$, as a function of λ, where D_{Cn} is the digital data of the light

intensity reflected from a substrate treated with $CH_3(CH_2)_{n-1}SH$. For all thiols, λ_0 is close to 500 nm. For a chain length $n < 12$, the contrast exhibits λ_{MIN} at about 490 nm and λ_{MAX} at about 520 nm. Conversely, for $n > 12$, the contrast exhibits λ_{MAX} at about 490 nm and λ_{MIN} at about 520 nm. The dependence of the contrast at both 490 and 520 nm on n is summarized in **Fig. 6(b)**. The contrast at 490 nm (520 nm) increases (decreases) monotonically with n. The non-zero contrast at 490 and 520 nm for $n = 11$ indicates that the C11 substrate can be distinguished from the C12 substrate via the contrast measurement. The image of the C11 substrate exhibits a different color from that of the C12 substrate (**Fig. S6**). Similarly, the contrasts at 490 and 520 nm for the C15 substrate are different from those of the C16 substrate. These results suggest that a unit of alkyl chain can be detected via the proposed method. The experimental data shown in **Figs. 6(a, b)** are supported by the calculated contrast values shown in **Fig. 6(c)**. The dotted black and gray curves in **Fig. 6(c)** correspond to the plots illustrated in **Fig. 6(b)**. The contrast at 490 nm certainly increases with n, whereas the opposite is true at 520 nm. Therefore, the number of alkyl chains can be simply identified from an image using a narrow band-pass filter by comparing it with the reference image.

The increase in the contrast with an increase of n is thought to be the mainly attributed to the alkyl chain length, not to the packing density and arrangement of the alkanethiol. The molecular structure of the alkanethiols (n = 2–22) adsorbed at a polycrystalline Au substrate has been investigated by ellipsometry.[41] In the research, the thickness of a monolayer above n = 10 increases linearly with an increase of n in contrast to n = 2–10. This suggests that alkanethiols assemble well with a tilt of ~25° from the surface normal by interlocking interactions of alkyl chains from a microscopic viewpoint. Therefore, the change in reflection intensity associated with the monolayer in the present study might be essentially related to the alkyl-chain-length as the averaged molecular structure of the assemblies.

Finally, the characteristics of the proposed method are described. Regarding height resolution, the method is mostly similar to optical interferometric microscopy, which has a height resolution of less than ~0.1 nm. Indeed, the microscopy measurements used in this study have been able to resolve differences of a unit in an alkyl chain, which corresponds to a height difference of 0.11 nm.[41, 42] However, an optical interferometric microscope is expensive, and the related images require complicated analysis. On the other hand, the proposed method enables the observation of characteristics which depend on differences of atomic order in height using a general optical microscope. Furthermore, the method permits the use of a simple commercial color digital camera instead of a monochrome cold camera (**Fig. S7**). In this study, a 5× objective lens was used, and the lateral resolution, limited by the objective lens, was approximately 2 μm. The use of an objective lens with a high magnification would improve the lateral resolution. However, it has been reported experimentally and theoretically that the large NA in the objective lens decrease the contrast by the influence of oblique illumination.[39, 40] Currently, the relationship between the lateral resolution and contrast is under investigation. Further theoretical model to visualize self-assembled monolayers on a metal film via optical microscopy is suggested.

CONCLUSIONS

A monolayer of *n*-alkanethiol with different chain lengths on a conductive Au thin film deposited onto a SiO_2/Si substrate was studied via ellipsometry and reflected light microscopy. Ellipsometry measurements of the substrates with and without a monolayer were found to yield optical properties depending on the presence of the monolayer. In addition, the optical properties of a C18 monolayer exhibited a large change compared with those of a C10 monolayer. The change in optical properties was also observed using a reflected light

microscope with a digital camera when two substrates, with and without the monolayer, were placed on the stage side by side. The change was evaluated on the basis of the contrast calculated from the digital data contained in a photograph acquired for the two substrates. The contrast, obtained using a narrow band-pass filter, was found to depend on the wavelength. This wavelength dependence was qualitatively supported by numerical calculations. The contrast exhibited maximum and minimum values at a certain wavelength. These values were found to change monotonically with the alkyl chain length of the monolayer. Therefore, reflected light microscope is a useful technique to identify the alkyl chain length of a monolayer formed on a thin Au film.

Although an Au thin film modified with alkanethiol on its entire surface was examined in this study, the proposed technique can be applied to the evaluation of the coverage for characterizing a monolayer or revealing the time evolution of its formation. Similarly, desorption of thiols via heat or ultraviolet light might also be detectable in the form of an endurance test for monolayers. Furthermore, the simultaneous observation of two substrates demonstrated in the study could be used to detect color differences between a sample and its reference. However, color differences can be detected from a single substrate by comparing the color change before and after surface treatment. This method might permit the visualization of the formation process or chemical reactions occurring on the substrate as they change with time, including applications in the field of bio sensing. The present microscopic technique will be useful for the construction of nanoscale structures via the bottom-up method not only for organic monolayers but also for inorganic ultra-thin films.

FIGURES

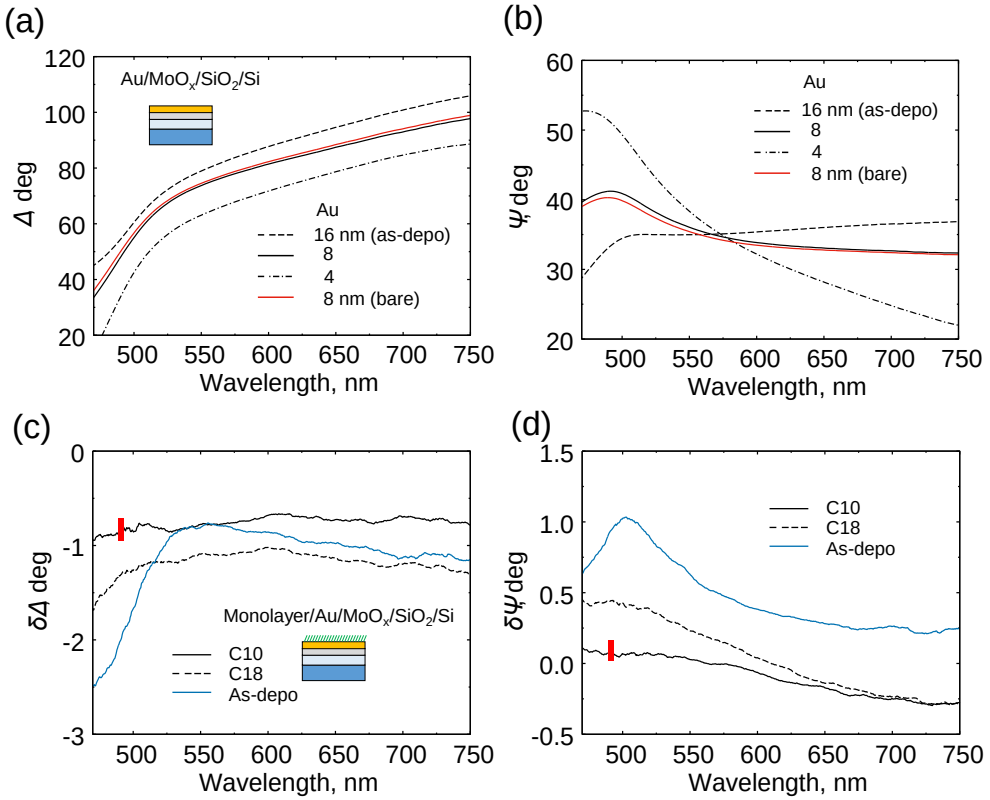

Figure 1 Ellipsometry spectra. **(a)** The phase difference, Δ and **(b)** amplitude ratio, Ψ correspond to substrates without a monolayer. The black dashed, solid, and dashed-dotted curves represent the as-deposited substrates with an Au thickness of 16, 8, and 4 nm, respectively. The red curves represent the substrate immersed in an ethanol solution without alkanethiol, which is defined as the bare substrate in this study. **(c)**, **(d)** The difference spectra, calculated as $\delta\Delta = \Delta_{\text{sample}} - \Delta_{\text{Au}}$ and $\delta\Psi = \Psi_{\text{sample}} - \Psi_{\text{Au}}$, respectively. Here, the subscripts "Au" and "sample" stand for the bare substrate and other substrates, respectively. The black solid, black dashed, and blue solid curves correspond to the 8-nm-thick Au substrates with C10, C18, and as-deposited, respectively. The red marks in the figures indicate the typical standard deviation of the measurement error.

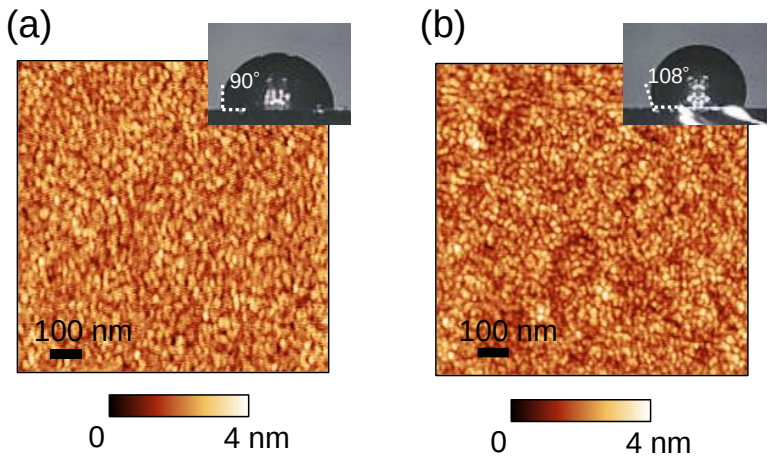

Figure 2 AFM images of the 8-nm-thick Au substrate surfaces for **(a)** the bare Au and **(b)** C18 substrate**.** The inset shows a water droplet on the surface for measurements of the contact angle.

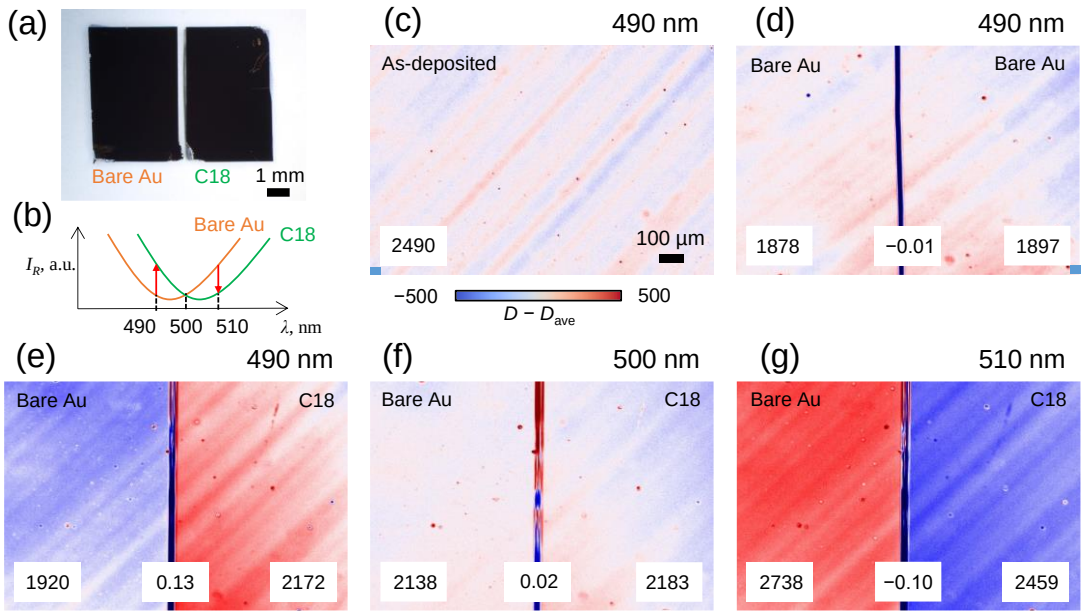

Figure 3 The optical microscopy images of the substrates. An 8-nm-thick Au substrate was cleaved into two pieces that were placed on the microscope stage side by side after surface treatment. **(a)** Photograph of the two substrates obtained from a substrate through cleavage. The formation of a monolayer can be confirmed via measurements of the water contact angle. **(b)** Schematic diagram of the reflection intensity as a function of the wavelength, showing the shift of the wavelength at which the reflection intensity is minimum. **(c–g)** Microscope images. A 12-bit image obtained from a digital camera cannot be expressed in general 8-bit image format; thus, an image is represented through its difference from the average of the 12-bit data with a color bar. The color and scale bar of **(c)** are applied to all images. **(c)** Image of an as-deposited substrate for λ = 490 nm. The number in the bottom-left corner is the average of the digital values in the image. **(d)** Image of the two pieces obtained from the bare Au substrate. The numbers in the bottom-left and bottom-right corners in the **(d–g)** panels represent the average for the substrate, whereas the number in the bottom-center part represents the contrast. The difference in the averages is about 1%. The influence of the cleavage is negligible. **(e–g)** Au and C18 substrates observed at λ = 490 **(e)**, 500 **(f)**, and 510 nm **(g)** in the same sample and same area. The magnitude relation of the average inverts at λ = ~500 nm.

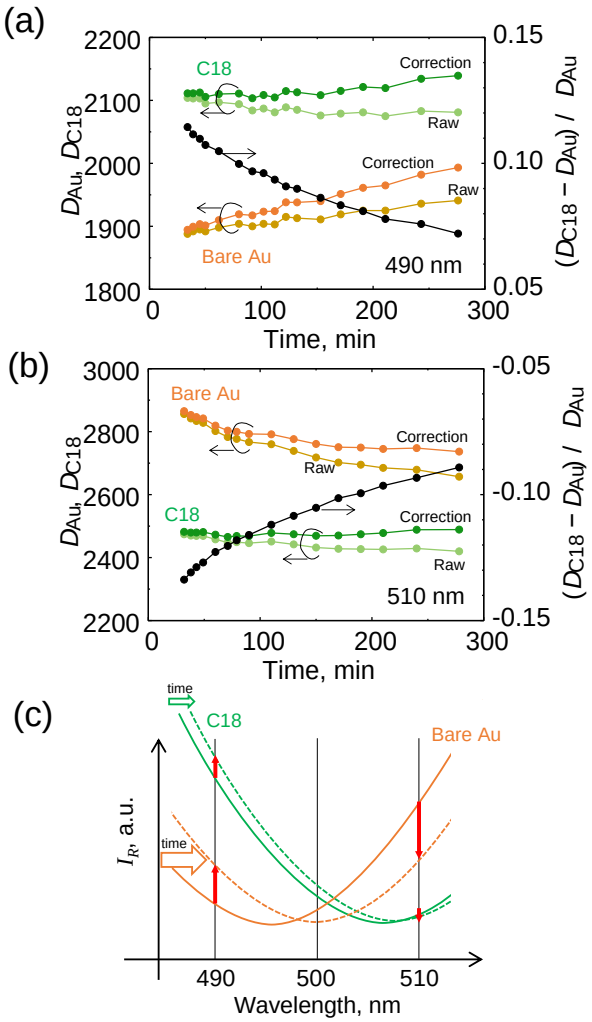

Figure 4 D_{Au} and D_{C18} as a function of time at λ = 490 nm **(a)** and 510 nm **(b)**. The gold (yellowish green) curves are the raw average of D for the bare Au (C18) substrate. The orange (green) curves are the average corrected from the raw value for the bare Au (C18) substrate. The black curve shows the contrast. **(c)** Schematic illustration of the shift of the I_R spectra, which might be attributed to adsorption of contamination on the substrate. The solid curves correspond to the initial state, just after surface modification. The minimum point gradually shifts toward higher wavelengths with time, resulting in the change of D with time. The shift for the bare Au substrate might be larger than that for the C18 substrate. The schematic is consistent with the experimental results.

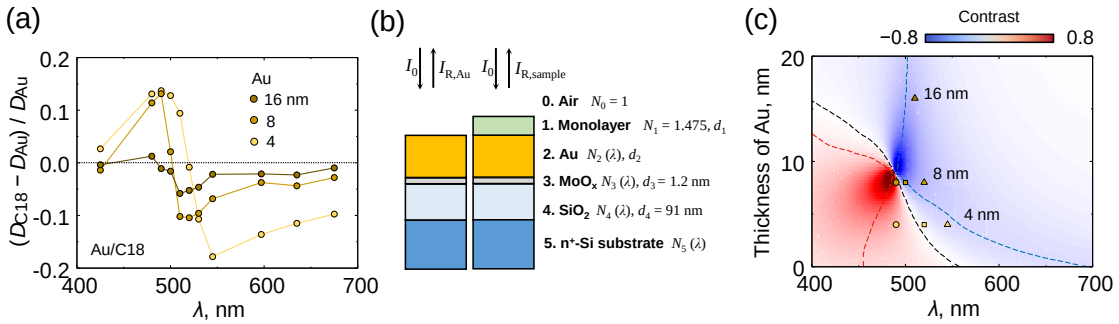

Figure 5 Contrast spectra for C18 substrates with different Au thickness. **(a)** Contrast spectra for the C18 substrates. **(b)** Calculation model. **(c)** Contour map of the contrast calculated as a function of the thickness of Au and λ. The dotted red, blue, and black curves correspond to the wavelength at which the contrast for the Au thickness is maximum, minimum, and zero, respectively. Circles, triangles, and squares are the experimental values obtained from the spectra in **(a)**.

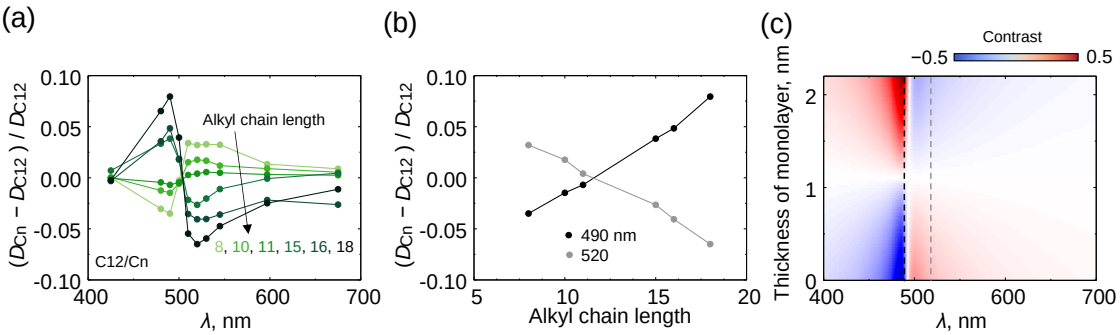

Figure 6 Contrast spectra of substrates having a monolayer with different alkyl chain lengths. C12 substrates are used as a reference instead of the bare Au substrate. **(a)** Contrast spectra for various alkyl chain lengths. **(b)** Contrast at λ = 490 and 520 nm as a function of the alkyl chain length. **(c)** Contrast calculated as a function of the monolayer thickness and λ, where the dotted black and gray curves represent the contrast at λ = 490 and 520 nm, respectively, compared with **(b)**. The monotonical increase in the experimental contrast at λ = 490 and 520 nm is qualitatively reproduced by calculations.

SUPPORTING INFORMATION

This supporting information provides the sheet resistance of the Au substrates, image correction for the background noise, calculation of the reflection intensity, microscopic images of the C11 and C12 substrates, and microscopic images acquired via the color camera.

AUTHOR INFORMATION

Corresponding Author

Email: *e-mail: hattori@eedept.kobe-u.ac.jp, **e-mail: kitamura@eedept.kobe-u.ac.jp

ORCID

Yoshiaki Hattori: 0000-0002-5400-8820

Masatoshi Kitamura: 0000-0003-1342-4796

Notes

The authors declare no competing financial interests.

ACKNOWLEDGMENT

This work was partly supported by a Leading Initiative for Excellent Young Researchers program from the MEXT in Japan, JSPS KAKENHI Grant Numbers 19H02171, 19K15048, Kawanishi Memorial ShinMaywa Education Foundation, and Kansai Research Foundation.

REFERENCES

(1) Love, J. C.; Estroff, L. A.; Kriebel, J. K.; Nuzzo, R. G.; Whitesides, G. M. Self-Assembled Monolayers of Thiolates on Metals as a Form of Nanotechnology. *Chem. Rev.* **2005**, *105*, 1103–1170.

(2) Flink, S.; van Veggel, F. C.; Reinhoudt, D. N. Sensor Functionalities in Self-Assembled Monolayers. *Adv. Mater.* **2000**, *12*, 1315–1328.

(3) Ho, P. K.; Granström, M.; Friend, R. H.; Greenham, N. C. Ultrathin Self-Assembled Layers at the ITO Interface to Control Charge Injection and Electroluminescence Efficiency in Polymer Light-Emitting Diodes. *Adv. Mater.* **1998**, *10*, 769–774.

(4) Yoshioka, T.; Fujita, H.; Kimura, Y.; Hattori, Y.; Kitamura, M. Wide-Range Work Function Tuning in Gold Surfaces Modified with Fluorobenzenethiols toward Application to Organic Thin-Film Transistors. *Flex. Print. Electron.* **2020**, *5*, 014011.

(5) Brandow, S. L.; Chen, M.-S.; Aggarwal, R.; Dulcey, C. S.; Calvert, J. M. Fabrication of Patterned Amine Reactivity Templates Using 4-Chloromethylphenylsiloxane Self-Assembled Monolayer Films. *Langmuir* **1999**, *15*, 5429–5432.

(6) Yam, C. M.; Kakkar, A. K. Molecular Self-Assembly of Dihydroxy-Terminated Molecules via Acid- Base Hydrolytic Chemistry on Silica Surfaces: Step-by-Step Multilayered Thin Film Construction. *Langmuir* **1999**, *15*, 3807–3815.

(7) Maury, P.; Escalante, M.; Reinhoudt, D. N.; Huskens, J. Directed Assembly of Nanoparticles onto Polymer-Imprinted or Chemically Patterned Templates Fabricated by Nanoimprint Lithography. *Adv. Mater.***2005**, *17*, 2718–2723.

(8) Sugimura, H.; Hozumi, A.; Kameyama, T.; Takai, O. Organosilane Self-Assembled Monolayers Formed at the Vapour/Solid Interface. *Surf. Interface Anal.* **2002**, *34*, 550–554.

(9) Takahashi, H.; Ikematsu, N.; Hattori, Y.; Kitamura, M. Formation of a Monolayer on a Gold Surface with High Thermal Stability Using Benzenedithiol. *Jpn. J. Appl. Phys.* **2019**, *59*, SDDA03.

(10) Tillman, N.; Ulman, A.; Schildkraut, J. S.; Penner, T. L. Incorporation of Phenoxy Groups in Self-Assembled Monolayers of Trichlorosilane Derivatives. Effects on Film Thickness, Wettability, and Molecular Orientation. *J. Am. Chem. Soc.* **1988**, *110*, 6136–6144.

(11) Angst, D. L.; Simmons, G. W. Moisture Absorption Characteristics of Organosiloxane Self-Assembled Monolayers. *Langmuir* **1991**, *7*, 2236–2242.

(12) Kang, B.; Park, N.; Lee, J.; Min, H.; Choi, H. H.; Lee, H. S.; Cho, K. Surface-Order Mediated Assembly of π-Conjugated Molecules on Self-Assembled Monolayers with Controlled Grain Structures. *Chem. Mater.* **2015**, *27*, 4669–4676.

(13) Onclin, S.; Mulder, A.; Huskens, J.; Ravoo, B. J.; Reinhoudt, D. N. Molecular Printboards: Monolayers of β-Cyclodextrins on Silicon Oxide Surfaces. *Langmuir* **2004**, *20*, 5460–5466.

(14) Li, D.; Swanson, B. I.; Robinson, J. M.; Hoffbauer, M. A. Porphyrin Based Self-Assembled Monolayer Thin Films: Synthesis and Characterization. *J. Am. Chem. Soc.* **1993**, *115*, 6975–6980.

(15) Vallant, T.; Brunner, H.; Mayer, U.; Hoffmann, H.; Leitner, T.; Resch, R.; Friedbacher, G. Formation of Self-Assembled Octadecylsiloxane Monolayers on Mica and Silicon Surfaces Studied by Atomic Force Microscopy and Infrared Spectroscopy. *J. Phys. Chem. B* **1998**, *102*, 7190–7197.

(16) Hoffmann, H.; Mayer, U.; Brunner, H.; Krischanitz, A. Reflection-Absorption Infrared Spectroscopy of Self-Assembled Monolayers on Gold and Silicon Surfaces. *Vib. Spectrosc.* **1995**, *8*, 151–157.

(17) Yokokawa, S.; Tamada, K.; Ito, E.; Hara, M. Cationic Self-Assembled Monolayers Composed of Gemini-Structured Dithiol on Gold: A New Concept for Molecular Recognition Because of the Distance between Adsorption Sites. *J. Phys. Chem. B* **2003**, *107*, 3544–3551.

(18) Wasserman, S. R.; Whitesides, G. M.; Tidswell, I. M.; Ocko, B. M.; Pershan, P. S.; Axe, J. D. The Structure of Self-Assembled Monolayers of Alkylsiloxanes on Silicon: A Comparison of Results from Ellipsometry and Low-Angle x-Ray Reflectivity. *J. Am. Chem. Soc.* **1989**, *111*, 5852–5861.

(19) Sugimura, H.; Ushiyama, K.; Hozumi, A.; Takai, O. Micropatterning of Alkyl-and Fluoroalkylsilane Self-Assembled Monolayers Using Vacuum Ultraviolet Light. *Langmuir* **2000**, *16*, 885–888.

(20) Lopez, G. P.; Biebuyck, H. A.; Whitesides, G. M. Scanning Electron Microscopy Can Form Images of Patterns in Self-Assembled Monolayers. *Langmuir* **1993**, *9*, 1513–1516.

(21) Hutter, E.; Fendler, J. H.; Roy, D. Surface Plasmon Resonance Studies of Gold and Silver Nanoparticles Linked to Gold and Silver Substrates by 2-Aminoethanethiol and 1, 6-Hexanedithiol. *J. Phys. Chem. B* **2001**, *105*, 11159–11168.

(22) Taglietti, A.; Fernandez, Y. A. D.; Galinetto, P.; Grisoli, P.; Milanese, C.; Pallavicini, P. Mixing Thiols on the Surface of Silver Nanoparticles: Preserving Antibacterial Properties While Introducing SERS Activity. *J. Nnanoparticle Res.* **2013**, *15*, 1–13.

(23) Nishiyama, K.; Tahara, S.; Uchida, Y.; Tanoue, S.; Taniguchi, I. Structural Differences in Self-Assembled Monolayers of Anthraquinone Derivatives on Silver and Gold Electrodes Studied by Cyclic Voltammetry and in Situ SERS Spectroscopy. *J. Electroanal. Chem.* **1999**, *478*, 83–91.

(24) Blake, P.; Hill, E. W.; Castro Neto, A. H.; Novoselov, K. S.; Jiang, D.; Yang, R.; Booth, T. J.; Geim, A. K. Making Graphene Visible. *Appl. Phys. Lett.* **2007**, *91*, 063124.

(25) Gorbachev, R. V.; Riaz, I.; Nair, R. R.; Jalil, R.; Britnell, L.; Belle, B. D.; Hill, E. W.; Novoselov, K. S.; Watanabe, K.; Taniguchi, T. Hunting for Monolayer Boron Nitride: Optical and Raman Signatures. *Small* **2011**, *7*, 465–468.

(26) Lee, G.-H.; Yu, Y.-J.; Lee, C.; Dean, C.; Shepard, K. L.; Kim, P.; Hone, J. Electron Tunneling through Atomically Flat and Ultrathin Hexagonal Boron Nitride. *Appl. Phys. Lett.* **2011**, *99*, 243114.

(27) Donnelly, G. E.; Velický, M.; Hendren, W. R.; Bowman, R. M.; Huang, F. Achieving Extremely High Optical Contrast of Atomically-Thin MoS2. *Nanotechnology* **2020**, *31* (14), 145706.

(28) Wanunu, M.; Vaskevich, A.; Rubinstein, I. Widely-Applicable Gold Substrate for the Study of Ultrathin Overlayers. *J. Am. Chem. Soc.* **2004**, *126*, 5569–5576.

(29) Ikematsu, N.; Takahashi, H.; Hattori, Y.; Kitamura, M. Formation of a Mixed Monolayer on a Gold Surface Using Fluorobenzenethiol and Alkanethiol. *Jpn. J. Appl. Phys.* **2019**, *59*, SDDA09.

(30) Prato, M.; Moroni, R.; Bisio, F.; Rolandi, R.; Mattera, L.; Cavalleri, O.; Canepa, M. Optical Characterization of Thiolate Self-Assembled Monolayers on Au (111). *J. Phys. Chem. C* **2008**, *112*, 3899–3906.

(31) Vos, M. F.; Macco, B.; Thissen, N. F.; Bol, A. A.; Kessels, W. M. M. Atomic Layer Deposition of Molybdenum Oxide from $(N^tBu)_2(NMe_2)_2Mo$ and O_2 Plasma. *J. Vac. Sci. Technol. A* **2016**, *34*, 01A103.

(32) Johnson, P. B.; Christy, R.-Wjp. Optical Constants of the Noble Metals. *Phys. Rev. B* **1972**, *6*, 4370–4379.

(33) Hattori, Y.; Kitamura, M. Crystal Orientation Imaging of Organic Monolayer Islands by Polarized Light Microscopy. *ACS Appl. Mater. Interfaces* **2020**, *12*, 36428–36436.

(34) Finklea, H. O.; Robinson, L. R.; Blackburn, A.; Richter, B.; Allara, D.; Bright, T. Formation of an Organized Monolayer by Solution Adsorption of Octadecyltrichlorosilane on Gold: Electrochemical Properties and Structural Characterization. *Langmuir* **1986**, *2*, 239–244.

(35) Velický, M.; Donnelly, G. E.; Hendren, W. R.; McFarland, S.; Scullion, D.; DeBenedetti, W. J. I.; Correa, G. C.; Han, Y.; Wain, A. J.; Hines, M. A.; Muller, D. A.; Novoselov, K. S.; Abruña, H. D.; Bowman, R. M.; Santos, E. J. G.; Huang, F. Mechanism of Gold-Assisted Exfoliation of Centimeter-Sized Transition-Metal Dichalcogenide Monolayers. *ACS Nano* **2018**, 12 (10), 10463–10472.

(36) Katzen, J. M.; Velický, M.; Huang, Y.; Drakeley, S.; Hendren, W.; Bowman, R. M.; Cai, Q.; Chen, Y.; Li, L. H.; Huang, F. Rigorous and Accurate Contrast Spectroscopy for Ultimate Thickness Determination of Micrometer-Sized Graphene on Gold and Molecular Sensing. *ACS Appl. Mater. Interfaces* **2018**, *10* (26), 22520–22528.

(37) Prato, M.; Alloisio, M.; Jadhav, S. A.; Chincarini, A.; Svaldo-Lanero, T.; Bisio, F.; Cavalleri, O.; Canepa, M. Optical Properties of Disulfide-Functionalized Diacetylene Self-Assembled Monolayers on Gold: A Spectroscopic Ellipsometry Study. *J. Phys. Chem. C* **2009**, *113*, 20683–20688.

(38) Uddin, M. J.; Hossain, M. K.; Hossain, M. I.; Qarony, W.; Tayyaba, S.; Mia, M. N. H.; Pervez, M. F.; Hossen, S. Modeling of Self-Assembled Monolayers (SAMs) of

Octadecanethiol and Hexadecanethiol on Gold (Au) and Silver (Ag). *Results Phys.* **2017**, *7*, 2289–2295.

(39) Casiraghi, C.; Hartschuh, A.; Lidorikis, E.; Qian, H.; Harutyunyan, H.; Gokus, T.; Novoselov, K. S.; Ferrari, A. C. Rayleigh Imaging of Graphene and Graphene Layers. *Nano Lett.* **2007**, *7*, 2711–2717.

(40) Huang, F. Optical Contrast of Atomically Thin Films. *J. Phys. Chem. C* **2019**, *123* (12), 7440–7446.

(41) Porter, M. D.; Bright, T. B.; Allara, D. L.; Chidsey, C. E. Spontaneously Organized Molecular Assemblies. 4. Structural Characterization of n-Alkyl Thiol Monolayers on Gold by Optical Ellipsometry, Infrared Spectroscopy, and Electrochemistry. *J. Am. Chem. Soc.* **1987**, *109*, 3559–3568.

(42) Skountzos, E. N.; von Wrochem, F.; Mavrantzas, V. G. Structure and Conformation of a Crystalline P3HT Film Adsorbed on an Alkanethiol Self-Assembled Monolayer Deposited on Gold. *Macromol. Theory Simul.* **2020**, *29*, 2000010.

Supporting Information for:

Chain-length Dependence of Optical Properties for an Alkanethiol Monolayer on an Ultra-thin Gold Film Revealed via Reflected Light Microscopy

Yoshiaki Hattori[†*], *Hayato Takahashi*[†], *Naoki Ikematsu*[†], *and Masatoshi Kitamura*[†**]

[†]Department of Electrical and Electronic Engineering, Kobe University, 1-1, Rokkodai-cho, Nada, Kobe, 657-8501, Japan

Corresponding author:
*e-mail: hattori@eedept.kobe-u.ac.jp, **e-mail: kitamura@eedept.kobe-u.ac.jp

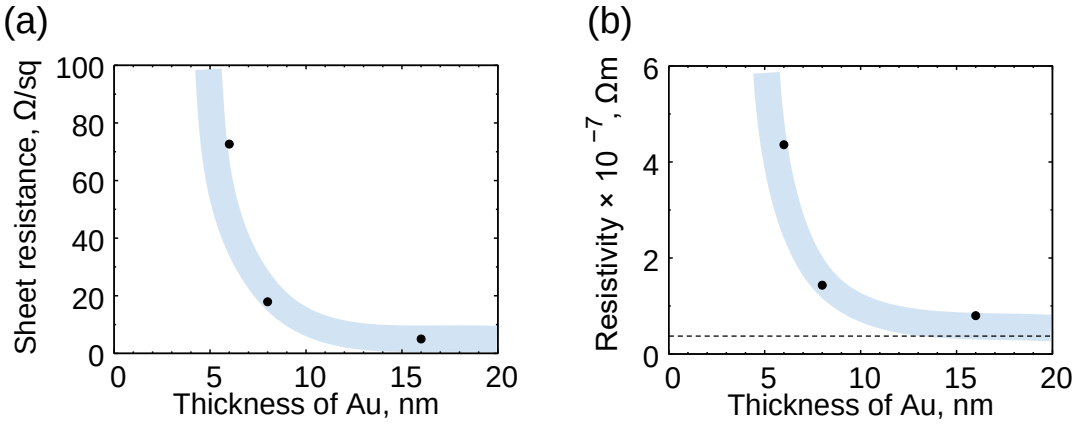

Figure S1: (a) Sheet resistance and **(b)** resistivity for the 6-, 8-, and 16-nm-thick Au substrate measured using the van der Pauw method. The resistivity is calculated by multiplying the sheet resistance by the thickness of the Au film. The light blue region in both figures is a guide for the eyes. The dotted curve in **(b)** is a typical resistivity for bulk Au. Both sheet resistance and resistivity decrease with the increase in thickness. The 4-nm-thick Au film is not conductive.

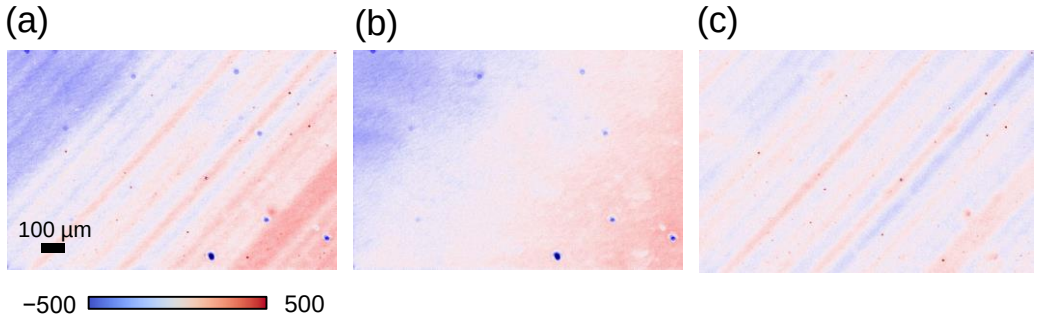

Figure S2: Image correction procedure for removing the background noise. **(a)** Original image of the 8-nm-thick Au substrate. **(b)** Reference image taken out of focus in the same area as for the substrate. A Gaussian blur was applied to the image for smoothing. **(c)** Corrected image obtained by subtracting the reference image from the original image. The three images display the difference in averaged digital values for each substrate with a color bar. The color and scale bar of **(a)** are also used for **(b)** and **(c)**.

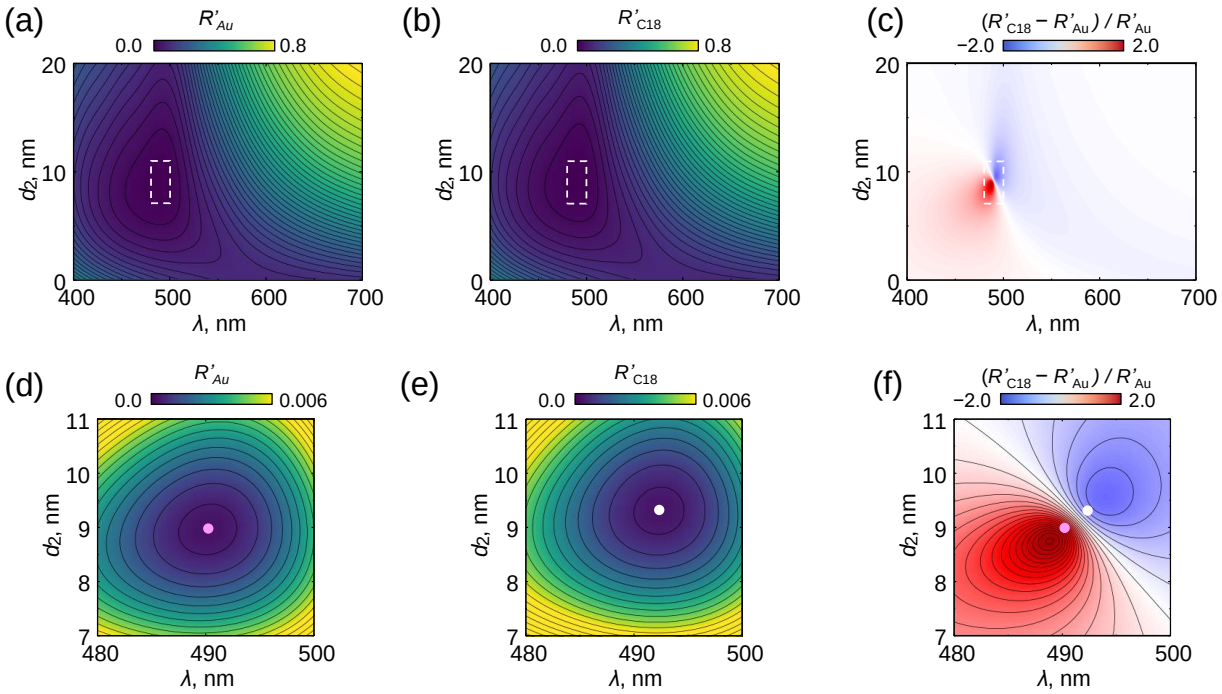

Figure S3: Numerical calculations of the reflected light intensity and contrast of the substrate. **(a)**, **(b)** Contour maps of R', obtained as a function of d_2 and λ, for the bare Au and C18 substrates, respectively. **(c)** Contour map of the contrast, defined as $(R'_{C18} - R'_{Au})/R'_{Au}$. **(d–f)** Enlarged maps of the area marked with a dashed white rectangle in **(a–c)**. Because of the interference in substrate, R' is weak at λ = ~500 nm in the bare Au substrate having an 8-nm-thick Au film. The pink dot in **(d)** shows the minimum point. When a C18 monolayer forms, the minimum point shifts toward a higher λ value and thicker Au direction, as shown by the white dot in **(e)**. The shift generates the color difference in the substrate. The pink and white points in **(f)** correspond to **(d)** and **(e)**, respectively. The maximum and minimum points of the contrast do not correspond to those of R'_{Au} and R'_{C18}. To enhance the visualization of a monolayer, large $|R'_{C18} - R'_{Au}|$ and small R'_{Au} values are required, as shown in **Fig. 3(b)**.

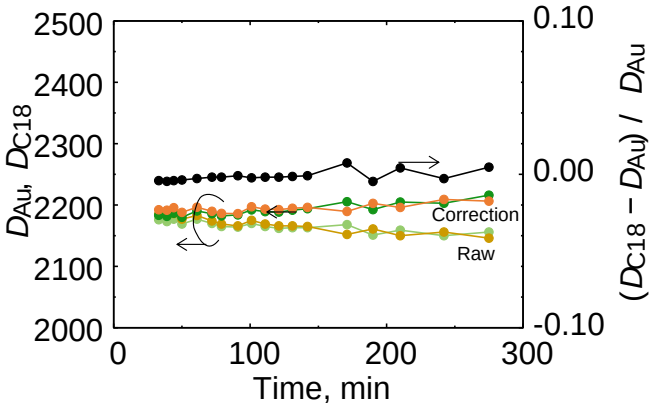

Figure S4: D_{Au} and D_{C18} as a function of time at λ = 500 nm. The gold (yellowish green) curve shows the raw averaged D value for the bare Au (C18) substrate. The orange (green) curve shows the corrected data for the bare Au (C18) substrate. The black curve shows the contrast. Through comparisons with **Fig. 4**, it can be seen that the change with time is small.

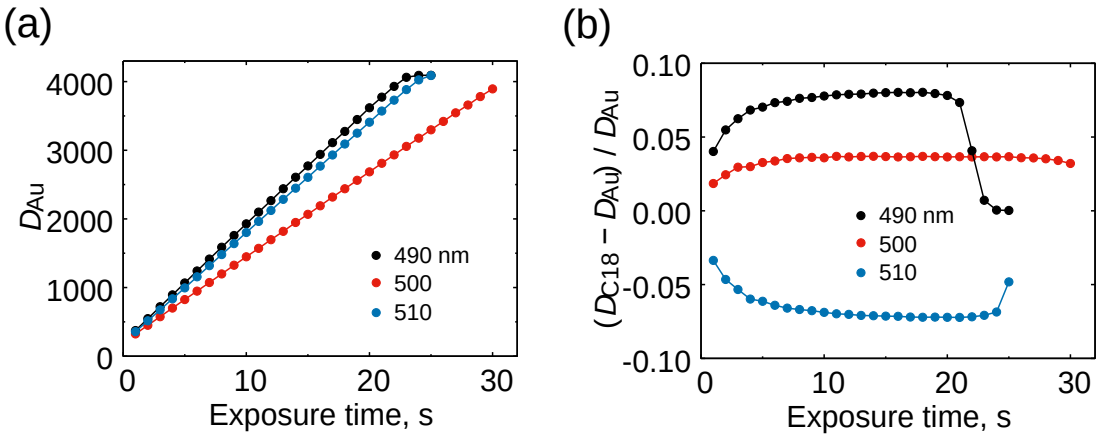

Figure S5: Influence of exposure time on contrast. **(a)** D_{Au} versus the exposure time for the 8-nm-thick Au substrate obtained at λ = 490, 500, and 510 nm. Ideally, D_{Au} linearly increases upon increasing the exposure time up to the maximum value ($4095 = 2^{14} - 1$). D_{Au} at λ = 500 nm is less than that at 490 and 510 nm. The dependence of D_{Au} on λ is explained by the interference in the layers. **(b)** Contrast for the C18 substrate at λ = 490, 500, and 510 nm as a function of the exposure time. The contrast is not constant. When the exposure time is short, the contrast is low because of the presence of the background noise. On the other hand, a long exposure time leads to the saturation of D, resulting in an inadequate condition for contrast. Therefore, the exposure time should be carefully determined based on the relationship between the contrast and exposure time. The appropriate exposure time for wavelengths of about 510 nm is approximately 15 s. The appropriate exposure time depends on the wavelength of the band-pass filter; this is because D strongly depends on the wavelength distribution of the light source and the characteristic of the band-pass filter, such as the FWHM, as well as the thickness of the Au film. Therefore, an appropriate exposure time should be determined for a substrate with a layer structure.

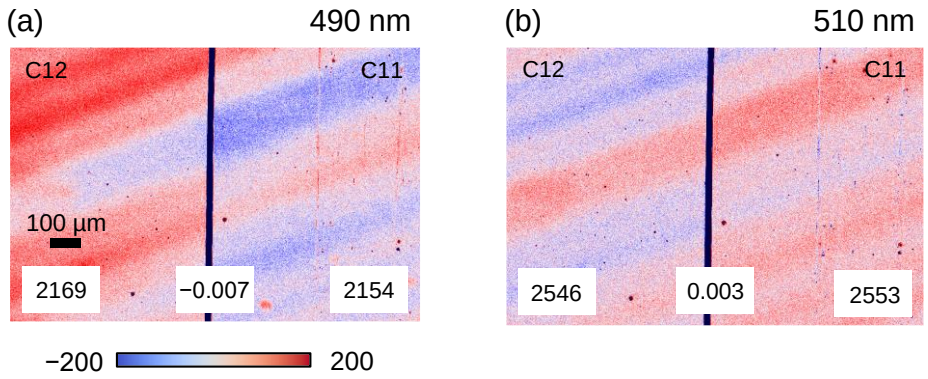

Figure S6: Microscope images for the C11 and a C12 substrates obtained at λ = 490 nm **(a)** and 510 nm **(b)**. The color and scale bar in **(a)** are the same as in **(b)**.

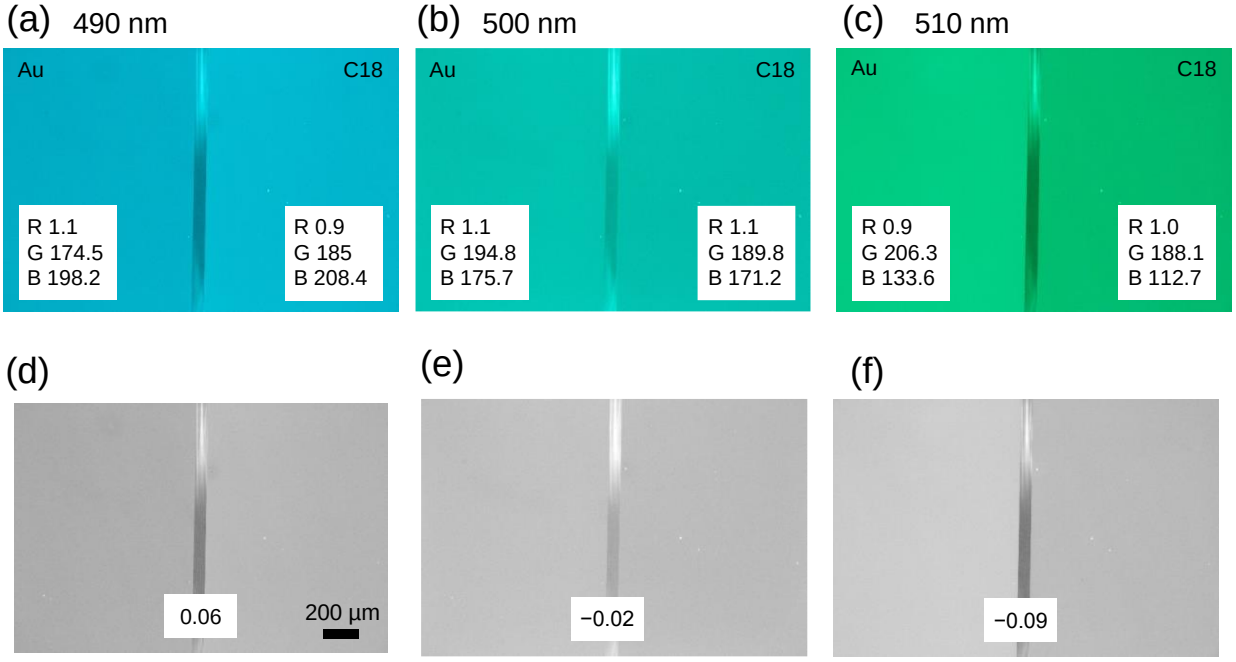

Figure S7: Microscopic images for the bare Au and C18 substrates taken using a commercial color digital camera. **(a–c)** color microscope images taken for the two substrates irradiated through a narrow band-pass filter at λ = 490, 500, or 510 nm. The same areas of the substrates were observed for **(a–c)**. The photographs were taken at the lowest ISO with auto shutter speed. The images shown here are the raw data. The average values of the 8-bit RGB values for the substrate are displayed in the bottom-left or bottom-right corners of the figures. **(d–f)** Grayscale images obtained from the G channel of **(a–c)**. The scale bar for **(d)** is applied to all images. The contrast calculated through the averaged G value is shown in the bottom-venter part of the figure and depends on λ. For **(d)**, the contrast is positive, and the right-hand side of the image is slightly brighter than the left-hand side. For **(e)**, the contrast is close to zero, and both sides have similar brightness. For **(f)**, the contrast is negative, and the right-hand side of the image is slightly darker than the left-hand side.